

A structure and energy dissipation efficiency of relativistic reconfinement shocks

Krzysztof Nalewajko^{*} and Marek Sikora

Nicolaus Copernicus Astronomical Center, Bartyleka 18, 00-716 Warsaw, Poland

3 November 2018

ABSTRACT

We present a semi-analytical hydrodynamical model for the structure of reconfinement shocks formed in astrophysical relativistic jets interacting with external medium. We take into account exact conservation laws, both across the shock front and in the zone of the shocked matter, and exact angular relations. Our results confirm a good accuracy of the approximate formulae derived by Komissarov & Falle (1997). However, including the transverse pressure gradient in the shocked jet, we predict an absolute size of the shock to be about twice larger. We calculate the efficiency of the kinetic energy dissipation in the shock and show a strong dependence on both the bulk Lorentz factor and opening angle of the jet.

Key words: galaxies: jets – shock waves.

1 INTRODUCTION

Geometry (cross-sectional size, opening angle, and bending) of supersonic, light jets is regulated, in general, by a complex system of oblique shocks. At certain circumstances they take form of reconfinement shocks (Sanders 1983). Such shocks have been considered to be responsible for non-thermal activity in AGN radio cores (see, *e.g.*, Daly & Marscher 1988; Komissarov & Falle 1997 – hereafter KF97; Stawarz *et al.* 2006) and, on much larger distances, in kiloparsec-scale radio knots (Komissarov & Falle 1998). They are also predicted to operate in massive X-ray binary systems (Perucho & Bosch-Ramon 2008) and in GRB collapsars (Bromberg & Levinson 2007).

A direct way to verify whether a given source can be interpreted in terms of a reconfinement shock is to determine whether location and extension of the source is consistent with a power of a jet and pressure/density of external medium. Under several simplifying assumptions analytical formulae relating these quantities were derived by Falle (1991) and, for relativistic shocks, by KF97. We have developed a semi-analytical model based on exact conservation laws and an exact dependence of a shock structure on an initial opening angle of a jet. Like in KF97, we adopt the cold jet approximation, *i.e.* we neglect the internal energy of the unshocked jet matter. The aim of this paper is to test the accuracy of the analytical formulae and to study the effects of including a transverse pressure gradients in the post-shock zone.

Our models are described in §2. They are compared with analytical results of KF97 in §3. We study the efficiency of energy dissipation in the reconfinement shocks in §4 and discuss their possible ‘astrophysical appearance’ in §5. Our main results are summarized in §6.

2 DESCRIPTION OF THE RECONFINEMENT MODELS

The models we develop here are stationary, axisymmetric and purely hydrodynamical. We use a cylindrical coordinate system originating at the central source, with z -axis aligned with the jet symmetry axis and r denoting the cylindrical radius. At every point, the flow is characterised by the following parameters: bulk Lorentz factor $\Gamma = 1/\sqrt{1-\beta^2}$, rest-density ρ , pressure p and the angle between the velocity vector and the z -axis θ . We use the equation of state for the ideal gas

$$p = (\gamma - 1)e, \quad (1)$$

where e is the internal energy density and γ is the numerical coefficient, which for non-relativistic and for ultra-relativistic gases coincides with the adiabatic index with a value 5/3 and 4/3, respectively. For intermediate cases and/or mixtures of non-relativistic and relativistic gases γ takes intermediate values which might somewhat differ from the respective values of the adiabatic indices (see KF97).

In a stationary flow conservation of mass, energy and momentum is expressed by the following equations:

$$\partial_i(\rho u^i) = 0, \quad (2)$$

^{*} E-mail: knalew@camk.edu.pl

3 GEOMETRICAL PROPERTIES OF RECONFINEMENT SHOCKS

The crucial characteristic of the reconfinement shocks is their length scale, which may be estimated observationally. KF97 provided simple analytic formulae, in which they connect geometrical properties of the shock surface to physical parameters, such as the external pressure p_e , the total power of a jet L_j , and its bulk Lorentz factor Γ_j . They assumed that: the pre-shock plasma is cold ($p_j \ll \rho c^2$); pressure behind the shock is equal to the external pressure ($p_s = p_e$); the half-opening angle Θ_j is small; and the pressure balance at the shock front, given by equation (15), can be approximated by the formula:

$$p_s = \mu u_j^2 \rho_j c^2 \sin^2(\theta_j - \alpha_s), \quad (21)$$

with $\mu = 17/24$.

Below, we rewrite their results, using slightly different notation. We launch the jet from the distance $z = z_0$. Let the external pressure profile be $p_e(z) = p_0(z/z_0)^{-\eta}$ (we expect $\eta \geq 0$). The shock surface should satisfy a boundary condition $r_s(z_0) = z_0 \tan \Theta_j$, where Θ_j is the jet half-opening angle. Then the shock surface equation is:

$$r_s(z) = \left[1 - \frac{z_0^{\eta/2}}{\delta \Lambda} (z^\delta - z_0^\delta) \right] \Theta_j z, \quad (22)$$

where $\delta = 1 - \eta/2$, and

$$\Lambda = \sqrt{\frac{\mu \beta_j L_j}{\pi p_0 c}}, \quad (23)$$

is a characteristic length scale¹. The reconfinement is found for $\eta < 2(1 + z_0/\Lambda)$ at

$$z_r = z_0 \left(1 + \delta \frac{\Lambda}{z_0} \right)^{1/\delta}. \quad (24)$$

The maximum width of unshocked jet,

$$r_m = \frac{z_0^2}{\Lambda} \left(\frac{z_r}{(1 + \delta)z_0} \right)^{1+\delta} \Theta_j, \quad (25)$$

is achieved at

$$z_m = \frac{z_r}{(1 + \delta)^{1/\delta}}. \quad (26)$$

The aspect ratio of the jet is given by

$$\frac{r_m}{z_r} = \frac{\delta + \frac{z_0}{\Lambda}}{(1 + \delta)^{1+\delta}} \Theta_j. \quad (27)$$

The shock surface inclination at z_0 is

$$\Theta_0 = \Theta_j \left(1 - \frac{z_0}{\Lambda} \right). \quad (28)$$

The half-closing angle (equal to minus the shock inclination at z_r) is

$$\Theta_r = \Theta_j \left(\delta + \frac{z_0}{\Lambda} \right). \quad (29)$$

¹ Note that in the Eq. (23) we have $\Lambda \propto L_j^{1/2} \beta_j^{1/2}$, while models of nonrelativistic jets predict $\Lambda \propto \tilde{L}_j^{1/2} \beta_j^{-1/2}$ (see Eq. (1) in Komissarov (1994) and refs. therein). The reason for the difference is that the term L_j includes the flux of the rest energy, $\dot{M}_j c^2$, while \tilde{L}_j doesn't.

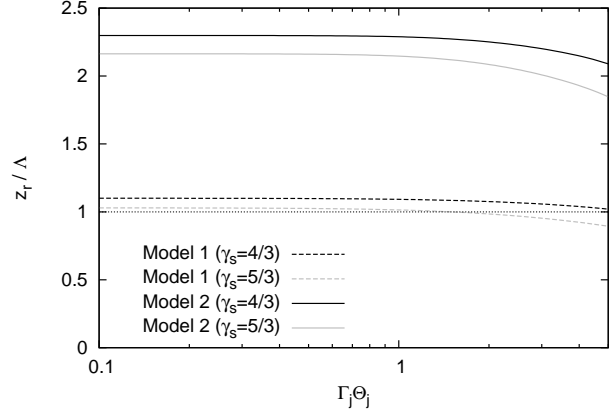


Figure 2. The ratio of reconfinement position z_r to the characteristic length Λ as a function of $\Gamma_j \Theta_j$. Results for Model 1 (dashed lines) and Model 2 (solid lines) are shown for different equations of state of the shocked matter: $\gamma_s = 4/3$ (black lines) and $\gamma_s = 5/3$ (grey lines).

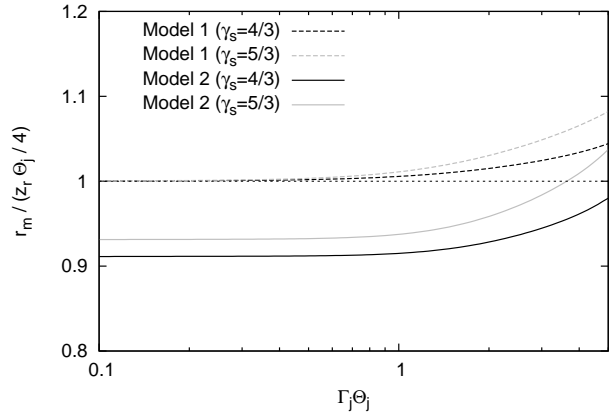


Figure 3. The aspect ratio of unshocked jet r_m/z_r , divided by the value $\Theta_j/4$ predicted by KF97, as a function of $\Gamma_j \Theta_j$. The linestyles are the same as in Fig. 2.

For the case of uniform external pressure ($\eta = 0$, $\delta = 1$) and a jet originating close to the central source ($z_0 \ll \Lambda$) we find the shock to be parabolic, with very simple characteristics: $z_r \simeq \Lambda$, $r_m/z_r \simeq \Theta_j/4$, $z_m \simeq z_r/2$, $\Theta_0 \simeq \Theta_r \simeq \Theta_j$. We have tested these relations in our two models, the results are shown on Figs. 2 – 5, as a function of half-opening angle Θ_j for a fixed $\Gamma_j = 10$. Other parameters used were $L_j = 10^{46} \text{ erg} \cdot \text{s}^{-1}$, $p_0 = 10^{-2} \text{ dyn}$ and $z_0 = 10^{15} \text{ cm}$. The characteristic length for these parameters is $\Lambda = 2.74 \cdot 10^{18} \text{ cm} = 0.89 \text{ pc}$.

A very good agreement between the results of Model 1 and the analytical formulae results from the same value of the pressure behind the shock ($p_s = p_e$). Deviations for $\Gamma_j \Theta_j > 1$ reflect the small angle approximation employed in analytical formulae. Small but systematic deviations of z_r from Λ result from approximate pressure balance equation.

In Model 2 the pressure behind the shock is systematically lower than p_e , but it cannot be fitted to a single power-law function of z . This results in longer reconfinement

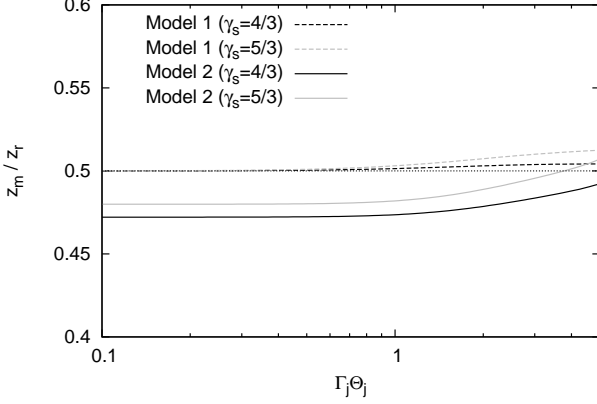


Figure 4. The ratio of the maximum jet width position z_m to the reconfinement position z_r as a function of $\Gamma_j \Theta_j$. The linestyles are the same as in Fig. 2.

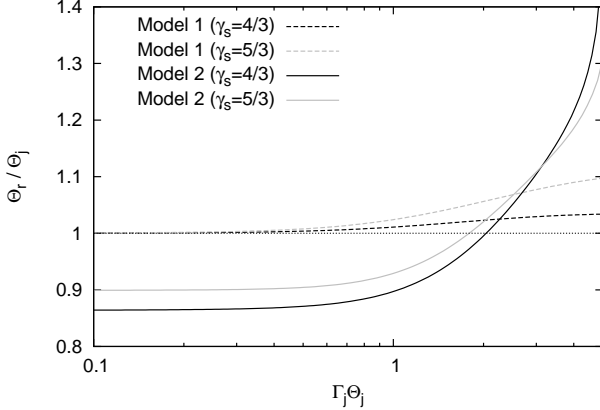


Figure 5. The ratio of the half-closing angle Θ_r to the half-opening angle Θ_j as a function of $\Gamma_j \Theta_j$. The linestyles are the same as in Fig. 2.

structures (by a factor of about 2.2). We have found that for small and intermediate half-opening angles: $r_m/z_r < \Theta_j/4$, $z_m < z_r/2$ and, accordingly, $\Theta_r < \Theta_j$. For large angles the deviations from analytical predictions are more pronounced. Nevertheless, the effects of independent values for the p_s are not particularly strong. The analytical formulae are still very useful within the order of magnitude accuracy.

4 ENERGY DISSIPATION

The kinetic energy flux through the shock front is dissipated with efficiency

$$\epsilon_{diss} \equiv \frac{F_{kin(j)} - F_{kin(s)}}{F_{kin(j)}} \quad (30)$$

where

$$F_{kin} \equiv \rho c^2 u_{\perp} (\Gamma - 1) \quad (31)$$

and u_{\perp} is the 4-velocity component normal to the shock front. Combining Eqs. (30), (31) and (14) gives

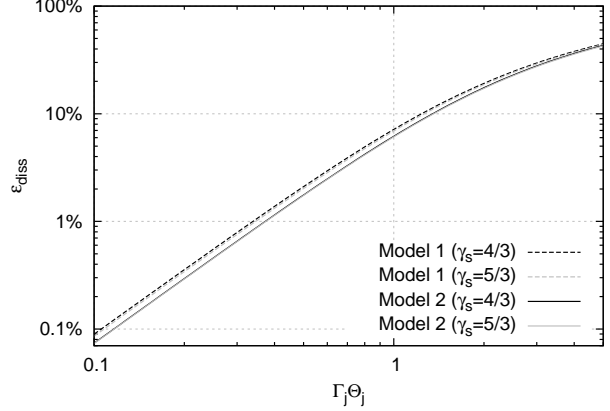


Figure 6. Dissipation efficiency ϵ_{diss} as a function of $\Gamma_j \Theta_j$, calculated for $\Gamma_j = 10$. The linestyles are the same as in Fig. 2.

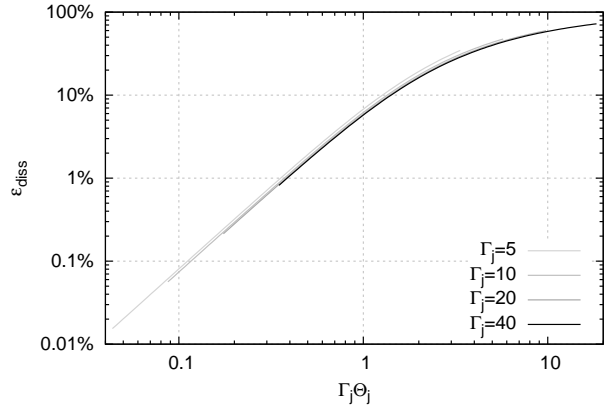


Figure 7. Dissipation efficiency ϵ_{diss} as a function of $\Gamma_j \Theta_j$, calculated for Model 2 with $\gamma_s = 4/3$. Line colour indicates the value of Γ_j : 5 (light grey), 10 (grey), 20 (dark grey) and 40 (black).

$$\epsilon_{diss} = \frac{\Gamma_j - \Gamma_s}{\Gamma_j - 1}. \quad (32)$$

As averaged over the entire shock front area, the efficiency of energy dissipation is found to strongly depend on the product $\Gamma_j \Theta_j$. Results for both models with a fixed $\Gamma_j = 10$ are shown in Fig. 6. We find that the averaged efficiency is very similar in both models and is insensitive to the value of γ_s . It approximately scales like $\epsilon_{diss} \sim 0.06(\Gamma_j \Theta_j)^2$ for $\Gamma_j \Theta_j < 1$, but its increase slows down at $\Gamma_j \Theta_j > 1$.

In order to determine whether ϵ_{diss} is truly a function of $\Gamma_j \Theta_j$, in Fig. 7 we present the results for Model 2 with $\gamma_s = 4/3$ and different values of Γ_j . We find little discrepancy between the curves, which implies that it is a well defined dependence.

We have investigated the z -profiles of the dissipated energy flux. In Fig. 8 we show the results for both models, with $\Gamma_j = 10$ and $\Theta_j = 5^\circ$. Although the reconfinement position z_r is more than twice large in Model 2, as compared to Model 1, the total amount of dissipated energy is very similar. The dissipated energy profiles have a well defined maximum, which we denote as $z_{diss,max}$. The ratio of $z_{diss,max}$ to z_r is shown in Fig. 9. It is larger in Model 1, but

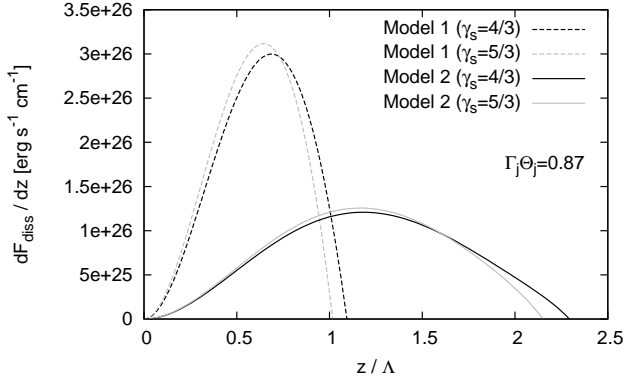


Figure 8. Profiles of dissipated energy flux produced at the shock surface, calculated for $\Gamma_j = 10$ and $\Theta_j = 5^\circ$. The linestyles are the same as in Fig. 2.

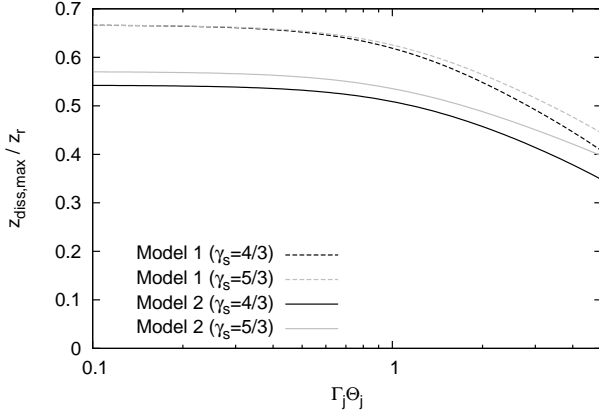


Figure 9. Ratio of the location of maximum of dissipated energy $z_{diss,max}$ to the reconfinement position z_r as a function of $\Gamma_j\Theta_j$. The linestyles are the same as in Fig. 2.

larger than $1/2$ in both models for $\Gamma_j\Theta_j < 1$. It decreases strongly with increasing $\Gamma_j\Theta_j$, for $\Gamma_j\Theta_j > 1$.

Noticing that the energy flux $F_w = w\Gamma u_\perp = (\rho c^2 + \gamma e)\Gamma u_\perp$ is conserved across the shock front (see Eq. 16), one can find that, for $\gamma_j \sim \gamma_s$, the efficiency of the internal energy production is

$$\epsilon_e \equiv \frac{F_{e(s)} - F_{e(j)}}{F_{kin(j)}} \sim \frac{1}{\gamma_s} \epsilon_{diss}. \quad (33)$$

A fraction of this energy is tapped by particles accelerated to relativistic energies and lost by nonthermal radiation. Such processes, if efficient, may significantly affect the shock structure.

It should be noted that in the case of particle acceleration with a broad energy distribution, most relativistic electrons may lose energy very efficiently even if the average energy dissipation efficiency is low. It means that, independently of the total energetics, the emissivity of such electrons will be maximized very close to the shock front and its spatial distribution will match the distribution of the energy dissipation.

5 ASTROPHYSICAL APPEARANCE

As theoretical analyses and numerical simulations demonstrate, formation of reconfinement shocks is accompanied by formation of reflection shocks (Sanders 1983; KF97). Furthermore, depending on a distribution of pressure or density of external medium, reconfinement and reflected shocks can form more or less abundant sequences of reconfinement shocks. Their radiative appearance is commonly modeled by assuming proportionality of the emissivity to the gas pressure (*e.g.* Gómez 2002; KF97). This leads to the predictions that most of the nonthermal radiation is produced around the reflection shocks. However, proportionality of the emissivity to the pressure is not what should be expected, if the efficiency of particle acceleration scales with the efficiency of energy dissipation. The latter is maximized at the shock fronts and, therefore, radiation emitted by most relativistic electrons will match geometrical structure of the shock fronts rather than the volume distribution of the pressure in the post shock flows. Of course, 'the shock front radiation' is likely to be accompanied by emission from the entire post-shock volume, by both slowly cooling lower energy electrons and by electrons accelerated in turbulent plasma in the 2nd order Fermi process. Specific geometrical and kinematical structures of reconfinement shocks are expected to be reflected in polarization properties, provided that magnetic fields are dominated by the shock compressed random field (Laing 1980; Cawthorne & Cobb 1990). This may explain perpendicular to the jet direction of polarization (EVPA) of radio knots in AGN kiloparsec scale jets (Bridle *et al.* 1994).

6 CONCLUSIONS

- Semi-analytical models were developed to calculate the structure of reconfinement shocks based on exact conservation laws and exact angular relations. The approximate analytical formulae of KF97, that describe a shape of the reconfinement shock and its dependence on the power of a jet and the pressure of external medium, were confirmed with a very good accuracy, even for $\Gamma_j\Theta_j$ up to a few. However, the absolute size of the structure is found to be larger by a factor about two, when including the transverse pressure gradient in the post-shock flow.

- The efficiency of energy dissipation in the relativistic reconfinement shocks scales approximately as $(\Gamma_j\Theta_j)^2$ for $\Gamma_j\Theta_j < 1$ and reaches about 6% at $\Gamma_j\Theta_j = 1$. For both models, with or without the transversal pressure gradients, the efficiency is very similar and for a given value of $\Gamma_j\Theta_j$ practically does not depend on the bulk Lorentz factor.

ACKNOWLEDGMENTS

The present work was partially supported by the Polish As-troparticle Network 621/E-78/SN-0068/2007.

REFERENCES

- Bridle, A. H., Hough, D. H., Lonsdale, C. J., Burns, J. O., & Laing, R. A., 1994, AJ, 108, 766

- Bromberg, O., & Levinson, A., 2007, ApJ, 671, 678, arXiv:0705.2040
- Cawthorne, T. V., & Cobb, W. K., 1990, ApJ, 350, 536
- Daly, R. A., & Marscher, A. P., 1988, ApJ, 334, 539
- Falle, S. A. E. G., 1991, MNRAS, 250, 581
- Gómez, J.-L., 2002, LNP, 589, 169, arXiv:astro-ph/0109338
- Komissarov, S. S., 1994, MNRAS, 266, 649
- Komissarov, S. S., & Falle, S. A. E. G., 1997, MNRAS, 288, 833 (KF97)
- Komissarov, S. S., & Falle, S. A. E. G., 1998, MNRAS, 297, 1087
- Laing, R. A., 1980, MNRAS, 193, 439
- Landau, L. D., & Lifshitz, E. M., 1959, Fluid Mechanics, Course of Theoretical Physics, Pergamon Press, Oxford
- Perucho, M., & Bosch-Ramon, V., 2008, A&A, 482, 917, arXiv:0802.1134
- Sanders, R. H., 1983, ApJ, 266, 73
- Stawarz, L., Aharonian, F., Kataoka, J., Ostrowski, M., Siemiginowska, A., & Sikora, M., 2006, MNRAS, 370, 981, arXiv:astro-ph/0602220

APPENDIX A: SOLVING THE SHOCK JUMP EQUATIONS

We show here a method by which the parameters of matter behind the shock may be determined in an exact analytical manner from equations (13 – 16). First, we express the angular parameters with non-angular ones. From equation (13) we find an expression for α_s , which is also a differential equation for the shock surface:

$$\tan \alpha_s = \frac{dr_s}{dz} = -\frac{\beta_s \cos \theta_s - \beta_j \cos \theta_j}{\beta_s \sin \theta_s - \beta_j \sin \theta_j} \quad (\text{A1})$$

From equations (14) and (A1), we find the deflection angle of velocity field:

$$\cos(\theta_s - \theta_j) = \frac{\Gamma_s \rho_s \beta_s^2 + \Gamma_j \rho_j \beta_j^2}{(\Gamma_s \rho_s + \Gamma_j \rho_j) \beta_s \beta_j} \quad (\text{A2})$$

Now we find two more equations for two unknown parameters: Γ_s , ρ_s :

$$\frac{w_s}{w_j} = \frac{\Gamma_j \rho_s}{\Gamma_s \rho_j} \quad (\text{A3})$$

$$(\Gamma_s^2 - \Gamma_j^2) \rho_s w_j = (p_j - p_s) \Gamma_s (\Gamma_s \rho_s + \Gamma_j \rho_j) \quad (\text{A4})$$

Equation (A3) is the result of dividing equation (16) by equation (14). Equation (A4) is derived from equation (15) by eliminating trigonometric functions using equations (13 – 14) and eliminating w_s using equation (A3). Using the equation of state for the shocked matter (and choosing the value of γ_s), we finally find from equations (A3) and (A4) a quadratic equation for Γ_s :

$$\begin{aligned} & [\gamma_s p_e (w_j - p_j + p_e)] \Gamma_s^2 + \\ & + [(\gamma_s - 1)(p_j - p_e) \rho_j c^2] \Gamma_j \Gamma_s + \\ & + [-w_j ((\gamma_s - 1)p_j + p_e)] \Gamma_j^2 = 0. \end{aligned} \quad (\text{A5})$$

Analyzing the parameters of this equation, we know that there is always only one positive solution. During our calculations, we set an alert for unphysical $\Gamma_s < 1$, but it never triggered. Finding Γ_s , we calculate ρ_s from equation (A4)

and then we find the angular parameters: θ_s from equation (A2) and α_s from equation (A1).

APPENDIX B: SOLVING THE EQUATIONS FOR CONSERVATION LAWS ACROSS THE SHOCKED ZONE

The normal vectors \vec{n}_s and \vec{n}_c are given explicitly by:

$$\vec{n}_s = -\cos \alpha_s \vec{e}_r + \sin \alpha_s \vec{e}_z, \quad (\text{B1})$$

$$\vec{n}_c = \cos \alpha_c \vec{e}_r - \sin \alpha_c \vec{e}_z. \quad (\text{B2})$$

Equations (19 – 20) may be expanded into:

$$\frac{d}{dz} \left[\int_{r_s}^{r_c} u \rho \cos \theta r dr \right] = (u_s \rho_s \sin \delta_s) \frac{r_s}{\cos \alpha_s}, \quad (\text{B3})$$

$$\frac{d}{dz} \left[\int_{r_s}^{r_c} \Gamma u w \cos \theta r dr \right] = (\Gamma_s u_s w_s \sin \delta_s) \frac{r_s}{\cos \alpha_s}, \quad (\text{B4})$$

$$\begin{aligned} \frac{d}{dz} \left[\int_{r_s}^{r_c} u^2 w \sin \theta \cos \theta r dr \right] = \\ = (u_s^2 w_s \sin \delta_s \sin \theta_s + p_s \cos \alpha_s) \frac{r_s}{\cos \alpha_s} - p_e r_c, \end{aligned} \quad (\text{B5})$$

$$\begin{aligned} \frac{d}{dz} \left[\int_{r_s}^{r_c} (u^2 w \cos^2 \theta + p) r dr \right] = \\ = (u_s^2 w_s \sin \delta_s \cos \theta_s - p_s \sin \alpha_s) \frac{r_s}{\cos \alpha_s} + p_e r_c \tan \alpha_c. \end{aligned} \quad (\text{B6})$$

To perform the integrals we have to describe the flow parameters between r_s and r_c as functions of r . We notice that the expressions to be integrated are linear functions of ρ and p (since the enthalpy w is also their linear function) and non-linear functions of Γ and θ . We decompose the integrated functions into $f(r) = g(\Gamma(r), \theta(r)) \cdot h(r) \cdot r$, where $h(r)$ is one of $\rho(r)$, $p(r)$ or $w(r)$. We assume that $h(r)$ is linear:

$$h(r) = h_s + \frac{h_c - h_s}{r_c - r_s} (r - r_s). \quad (\text{B7})$$

The integrals are approximated with

$$\int_{r_s}^{r_c} f dr \simeq \frac{g(\Gamma_s, \theta_s) + g(\Gamma_c, \theta_c)}{2} \int_{r_s}^{r_c} h(r) r dr. \quad (\text{B8})$$

Substituting these formulae to equations (B3 – B6) we obtain a system of 4 differential equations for 8 variables: Γ_s , ρ_s , θ_s , α_s , p_s , Γ_c , ρ_c and α_c . The system is then closed by including differential forms of equations (13 – 16).